

A Semantics-Aware Hierarchical Self-Supervised Approach to Classification of Remote Sensing Images

Giulio Weikmann, Gianmarco Perantoni, and Lorenzo Bruzzone, *Fellow, IEEE*

Abstract—Deep learning has become increasingly important in remote sensing image classification due to its ability to extract semantic information from complex data. Classification tasks often include predefined label hierarchies that represent the semantic relationships among classes. However, these hierarchies are frequently overlooked, and most approaches focus only on fine-grained classification schemes. In this paper, we present a novel Semantics-Aware Hierarchical Consensus (SAHC) method for learning hierarchical features and relationships by integrating hierarchy-specific classification heads within a deep network architecture, each specialized in different degrees of class granularity. The proposed approach employs trainable hierarchy matrices, which guide the network through the learning of the hierarchical structure in a self-supervised manner. Furthermore, we introduce a hierarchical consensus mechanism to ensure consistent probability distributions across different hierarchical levels. This mechanism acts as a weighted ensemble being able to effectively leverage the inherent structure of the hierarchical classification task. The proposed SAHC method is evaluated on three benchmark datasets with different degrees of hierarchical complexity on different tasks, using distinct backbone architectures to effectively emphasize its adaptability. Experimental results show both the effectiveness of the proposed approach in guiding network learning and the robustness of the hierarchical consensus for remote sensing image classification tasks.

Index Terms—Consensus, deep learning (DL), hierarchical, multi-level agreement, self-supervision, semantics-aware, Sentinel-2, time series, multispectral, very high resolution, remote sensing

I. INTRODUCTION

IMAGE classification and semantic segmentation are fundamental tasks in image processing. While Deep Learning (DL) methods have significantly advanced the field by learning powerful feature representations, standard approaches often treat classification as a flat, single-level task. However, many applications involve target categories having a natural

hierarchical structure, exhibiting multiple levels of semantic granularity (e.g., object taxonomies, language, land-cover systems) [1]–[3]. Neglecting this inherent structure discards valuable semantic information and can lead to suboptimal or inconsistent predictions [4]. This is particularly relevant when dealing with label ambiguity or variations in image quality (such as resolution or artifacts) that may only permit reliable classification at coarser semantic levels.

A key challenge is integrating hierarchical information effectively into the learning process. Traditional methods frequently rely on post-processing steps or fixed rule-based systems to enforce hierarchical consistency, which limit their ability to learn complex, data-driven relationships between levels [5]–[8]. Furthermore, constructing large-scale datasets with consistent multi-level annotations is often difficult [9], [10]. This requires methods capable of handling data labelled at various levels within the hierarchy. Although standardized hierarchical classification schemes exist in several domains, e.g., COOrdination of INformation on the Environment (CORINE) and Land Cover Classification System (LCCS) in Remote Sensing (RS), most current DL models do not explicitly leverage this structure during training.

Most hierarchical approaches focus on extracting features at multiple levels of granularity without explicitly modeling the hierarchical relationships intrinsic to the task [11], [12]. This poses a limitation, as the hierarchy arises from the problem domain itself rather than from specific architectural design choices. Accordingly, an effective hierarchical learning principle should be generalizable and scalable across different DL architectures. However, existing methods often produce non-modular architectures with rigid structures, thereby limiting the flexibility in the DL backbone selection.

In this paper, we propose a novel image processing methodology to modularly improve scene classification and semantic segmentation through semantic relationships across categories. Our approach leverages the hierarchical structure of standardized classification schemes by introducing a classification head for each hierarchical level. We further introduce trainable hierarchy matrices to model the relationships between these levels. To enforce consistency across the hierarchy, we define a multi-level consensus prediction that promotes agreement among the predictions at different levels. Additionally, we introduce a self-supervised consensus loss that implicitly learns the hierarchical relationships within the data. This approach allows the discovery of intricate semantic relationships that can deviate from the simple user-defined aggregation rules, leading

This work was partially supported by European Space Agency (ESA) Climate Change Initiative (CCI+) New Essential Climate Variables (ECVs) High Resolution Land Cover (HRLC), under Contract 4000125259718/I-NB and partially supported by the Italian Space Agency (ASI) and the Ministry of University and Research (MUR) under Contract 2024-5-E.0 - CUP n. I53D24000060005, by the Project "Space It Up!". (*Corresponding author: Lorenzo Bruzzone.*)

Giulio Weikmann, Gianmarco Perantoni and Lorenzo Bruzzone are with the Department of Information Engineering and Computer Science, University of Trento, 38123 Trento, Italy (e-mail: giulio.weikmann@unitn.it; gianmarco.perantoni@unitn.it; lorenzo.bruzzone@unitn.it).

This work has been submitted to the IEEE for possible publication. Copyright may be transferred without notice, after which this version may no longer be accessible.

to improved classification accuracy and semantic consistency. We demonstrate the effectiveness of our approach on different RS image classification tasks, including semantic segmentation of Satellite Image Time Series (SITS) of multispectral acquisitions and Very-High Resolution (VHR) RS scene classification tasks.

The key contributions of this work can be summarized as follows:

- 1) We define a hierarchical image processing approach to semantic segmentation and scene classification that integrates multi-level classification modules with DL backbones, along with trainable projection matrices to model hierarchical semantic relationships.
- 2) We propose a novel self-supervised consensus loss function that enforces consistency across different hierarchical levels, enhancing the semantic coherence of the classification results.
- 3) The proposed method is general and can be applied to any DL architecture and hierarchical classification scheme, offering flexibility in defining architecture details.
- 4) We demonstrate the effectiveness of the proposed approach on three RS datasets that include images with varying resolutions and different complexities in their hierarchical relationships.

The remainder of this paper is organized as follows. Section II reviews related works on hierarchical semantic segmentation. Section III details the proposed hierarchical consensus approach. The datasets and experimental setup are described in Section IV, while Section V presents and discusses the experimental results. Finally, Section VI concludes the paper and outlines future research directions.

II. RELATED WORKS

Image classification is a fundamental task in computer vision and image processing, with DL models achieving state-of-the-art performance across various domains. Standard approaches typically treat classification as a “flat” problem in a traditional single-granularity classification, predicting probabilities over a set of mutually exclusive classes without explicitly considering potential semantic relationships or hierarchical structures among them. However, many real-world datasets possess inherent taxonomies where classes can be organized into hierarchies (*e.g.*, species classification, object recognition with super-/sub-categories). Ignoring this structure can lead to suboptimal performance, as the model is not able to leverage prior knowledge about class relationships. Consequently, standard loss functions inherently treat all misclassifications equally. Without an explicit hierarchical representation, they fail to differentiate between errors involving closely related classes and those involving semantically distant ones.

Leveraging hierarchical label structures during model training and inference has emerged as a promising direction to improve accuracy and semantic understanding. Early work demonstrated that standard Convolutional Neural Networks (CNNs) implicitly capture some hierarchical information, with shallower layers grouping high-level categories and deeper

layers specializing in finer distinctions [13]. Building on this, researchers have explored explicit methods to incorporate hierarchy. Typically, this is achieved by mapping the label hierarchy to network architectures or by introducing loss functions that handle the hierarchical correlation between different granularity tasks [14]–[16]. Bertinetto *et al.* [17] proposed a level-wise hierarchical cross-entropy loss based on conditional probabilities within the hierarchy and used mapping functions to embed class relationships. Similarly, Garg *et al.* [18] introduced the Hierarchy Aware Features (HAF), incorporating multiple losses, including minimizing the Jensen-Shannon Divergence (JSD) between aggregated predictions at different hierarchy levels and enforcing geometric consistency in the feature space, aiming to reduce the severity of misclassifications. In [19], the authors proposed hierarchy and exclusion graphs to model semantic relations between two labels assigned to the same objects. They considered exclusions, overlaps, and subsumptions, and provided a detailed theoretical analysis of the structure of the hierarchical problem. Building on this work, a combinatorial loss is proposed in [20], which addresses the scenario where samples might be labelled at different levels of granularity. The loss is designed to maximize the marginal probability of the observed ground truth label by aggregating information from related labels in the hierarchy. The authors introduced a Hierarchical Residual Network (HRN) architecture, where features from parent levels act as residual connections to inform child-level features, explicitly facilitating hierarchical feature interaction.

While these methods demonstrate the benefits of hierarchy-aware learning, they often rely on the assumption that a predefined and accurate hierarchy is available, where no hierarchy violation is possible. This assumption may not hold in all scenarios, as real-world taxonomies can be noisy, incomplete, or subjective. Furthermore, many existing techniques require explicit guidance or architectural modifications tailored to a specific fixed hierarchy [21], potentially limiting their flexibility and ability to adapt if the underlying hierarchical understanding evolves or is uncertain. For example, some approaches decompose the problem into sequential decisions or binary classifications guided by the known structure [21]–[23], rather than allowing the model to learn or refine hierarchical relationships implicitly from the data. The challenge remains to develop methods that can effectively exploit hierarchical semantics, even when the hierarchy is imperfect, labels are provided at varying granularity levels, or needs to be partially inferred in a robust and data-driven manner.

III. PROPOSED METHODOLOGY

In this work, we address the above-mentioned challenges by proposing a novel deep learning framework for hierarchy-aware image classification. Our approach models the hierarchical semantic relationships within image data by integrating hierarchical loss components with a robust consensus mechanism. This allows the model to leverage potential hierarchical structures effectively while mitigating the impact of potential inaccuracies or inconsistencies in the predefined taxonomy. Specifically, our method aims to learn and exploit hierarchical

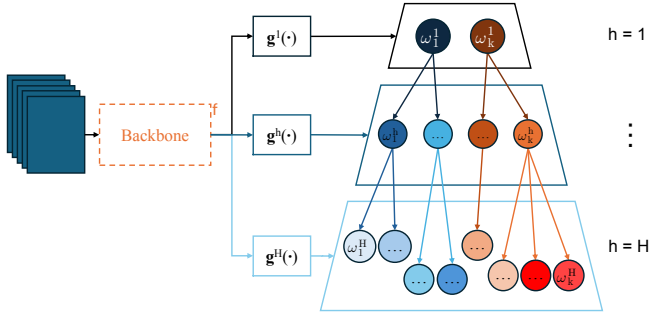


Fig. 1. Overview of the proposed hierarchical structure within the backbone (left) and associated hierarchical label tree (right). Different classification modules are trained to classify different hierarchical levels from the features extracted by the backbone.

relationships in a more implicit, self-supervised fashion within a hierarchy-aware architecture, reducing the reliance on rigid, externally defined structure.

A. Hierarchical Problem Formulation

Let us denote column vectors by lowercase bold letters (*e.g.*, \mathbf{v}) and matrices by uppercase bold letters (*e.g.*, \mathbf{B}). The i th component of a vector \mathbf{v} is denoted by v_i , while the i th row and j th column of a matrix \mathbf{B} are denoted by $\mathbf{B}_{i,\cdot}$ and $\mathbf{B}_{\cdot,j}$, respectively. Then, let us consider a user-defined hierarchy label tree with H levels, where the leaves represent the finest level of detail. We denote each hierarchical level as $h \in [1, 2, \dots, H]$, ranging from the coarsest level $h = 1$ to the finest one $h = H$. The root node $h = 0$ is not considered, as it represents the trivial case in which all classes are mapped into a single class. Let $\mathbf{x} \in \mathbb{R}^b$ be the input vector, where b is the number of input features. Its associated labels are $y^h \in \Omega^h$, where $\Omega^h = \{\omega_1^h, \dots, \omega_{|\Omega^h|}^h\}$ is the set of labels at hierarchical level h , with $|\Omega^h|$ number of labels. For every $h_1 < h_2$, we have that each fine-grained class $\omega_j^{h_2}$ is mapped to a coarse-grained class $\omega_i^{h_1}$, and $|\Omega^{h_1}| < |\Omega^{h_2}|$. We define this mapping relationship by $\omega_j^{h_2} \implies \omega_i^{h_1}$. Let $\mathcal{D} = \{(\mathbf{x}_n, Y_n) | n = 1, \dots, N\}$ be the training set, where for each input feature vector \mathbf{x}_n , we have an associated set $Y_n = \{y_n^1, \dots, y_n^h, \dots, y_n^H\}$, which denotes the ground truth labels at all H hierarchical levels, for a total number of N training samples. The labels in the dataset satisfy a nested label structure, where each class at a finer level is contained within a class at a coarser level.

B. Fully-Supervised Multi-Level Learning

The proposed methodology can be applied to any backbone network by simply introducing the required additional hierarchical classification modules. We refer to each of the hierarchical classification modules $\mathbf{g}^h : \mathbb{R}^d \rightarrow \mathbb{R}^{|\Omega^h|}$ on top of a given backbone network as the composition $\mathbf{g}^h \circ \mathbf{f} : \mathbb{R}^b \rightarrow \mathbb{R}^{|\Omega^h|}$, where $\mathbf{f} : \mathbb{R}^b \rightarrow \mathbb{R}^d$ is the backbone feature extractor. Fig. 1 provides a high-level overview of the considered multi-level classification approach.

Each classifier \mathbf{g}^h estimates class-posterior logits. Let $\hat{\mathbf{p}}^h(\mathbf{x}) \in \mathbb{R}^{|\Omega^h|}$ be the vector of estimated class-posterior probabilities at level h given \mathbf{x} , *i.e.*, $\hat{\mathbf{p}}^h(\mathbf{x}) = [\hat{P}(\omega_1^h | \mathbf{x}), \dots, \hat{P}(\omega_{|\Omega^h|}^h | \mathbf{x})]^\top$, where \top refers to the transpose operator. Then, the class-posterior probabilities $\hat{\mathbf{p}}^h$ for the input sample \mathbf{x} at level h can be retrieved as follows:

$$\hat{\mathbf{p}}^h(\mathbf{x}) = \sigma[\mathbf{g}^h(\mathbf{f}(\mathbf{x}))], \quad (1)$$

where $\sigma : \mathbb{R}^d \rightarrow [0, 1]^d$ is the *softmax* operator, with $\sigma_i[\cdot]$ computed as follows:

$$\sigma_i[\mathbf{g}] = \frac{\exp g_i}{\sum_j \exp g_j} \in [0, 1]. \quad (2)$$

The training of \mathbf{g}^h is done by computing the categorical cross-entropy (CCE) loss as follows:

$$\begin{aligned} \mathcal{L}_{CCE}^h &= -\frac{1}{N} \sum_{n=1}^N \sum_{i=1}^{|\Omega^h|} \mathbb{1}[y_n^h = \omega_i^h] \log \hat{P}^h(\omega_i^h | \mathbf{x}_n) \\ &= -\frac{1}{N} \sum_{n=1}^N \sum_{i=1}^{|\Omega^h|} \mathbb{1}[y_n^h = \omega_i^h] \log \sigma_i[\mathbf{g}^h(\mathbf{f}(\mathbf{x}_n))], \end{aligned} \quad (3)$$

where $\mathbb{1}[\cdot]$ serves as an indicator function and takes a value of one when the argument is true, else zero. We apply the CCE loss function to all hierarchical levels, obtaining the total CCE loss \mathcal{L}_{CCE} as the sum of the level-wise losses:

$$\mathcal{L}_{CCE} = \sum_{h=1}^H \lambda^h \mathcal{L}_{CCE}^h. \quad (4)$$

As it has also been noted in previous works [24], adopting several CCE loss functions for diverse classification levels may negatively affect performance at the most granular classification level. To mitigate this behavior, we introduced the weighting terms $\lambda = \{\lambda^1, \dots, \lambda^H\}$ to limit the impact of coarser levels, while still accounting for the additional losses.

C. Hierarchy Matrices

The CCE loss functions at each hierarchical level lead to independent classifications, which are not constrained to follow the hierarchy definition formulated in the problem statement. To impose the hierarchical constraints, additional consensus predictions and self-supervised penalty terms are introduced. These penalty terms are defined through hierarchy projection matrices designed to map the correct relationships between the different layers.

Let us consider for simplicity the case of $H = 2$ levels, with h_1 representing the coarse-grained labels and h_2 the fine-grained labels, *i.e.*, $h_1 < h_2$. We refer to Ω^{h_1} as the set of the *macroclasses* (*i.e.*, the coarse-grained classes) and to Ω^{h_2} as the set of the *microclasses* (*i.e.*, the fine-grained classes). We can define the hierarchy indicator matrix $\mathbf{I}^{h_2, h_1} \in \{0, 1\}^{|\Omega^{h_2}| \times |\Omega^{h_1}|}$, which represents the hierarchical relationship between level h_2 and h_1 :

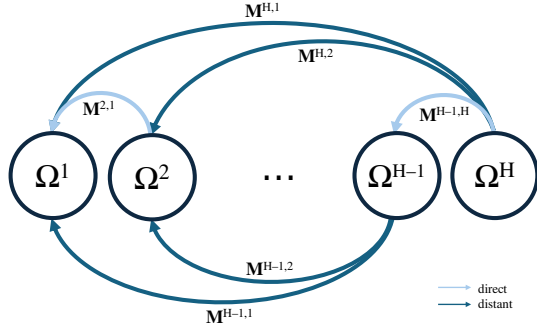


Fig. 2. Illustration of both direct and distant hierarchical mappings, from fine-grained classes to coarse-grained classes.

$$\mathbf{I}^{h_2, h_1} = \begin{bmatrix} I_{1,1} & I_{1,2} & \cdots & I_{1,|\Omega^1|} \\ I_{2,1} & I_{2,2} & \cdots & I_{2,|\Omega^1|} \\ \vdots & \vdots & \ddots & \vdots \\ I_{|\Omega^2|,1} & I_{|\Omega^2|,2} & \cdots & I_{|\Omega^2|,|\Omega^1|} \end{bmatrix}. \quad (5)$$

This approach can be easily extended to a multi-level scenario, considering any given number H of hierarchical levels. In this case, the total number of hierarchy matrices that can be determined is $((H-1) \cdot H)/2$, as also mappings of distant relationship levels can be defined (e.g., from the root of the label tree to the leaves, skipping intermediate levels) if needed. An example is illustrated in Fig. 2. The hierarchy indicator matrices are initialized with ones and zeros representing the user-defined mapping. Consequently, $I_{i,j}^{h_2, h_1}$ assumes a value of one when the microclass $\omega_i^{h_2}$ is contained in the macroclass $\omega_j^{h_1}$ through the relationship $\omega_i^{h_2} \implies \omega_j^{h_1}$, thus defining the matrix elements as follows:

$$I_{i,j}^{h_2, h_1} = \begin{cases} 1 & \text{if } \omega_i^{h_2} \implies \omega_j^{h_1} \\ 0 & \text{otherwise} \end{cases}. \quad (6)$$

It is important to note that, in the case of hard-hierarchies, each microclass corresponds to exactly one macroclass. However, this may not hold true as there might exist semantic overlaps in the hierarchy structure. Additionally, a distinction between *user-defined* aggregations and *data-driven* aggregations has to be made. While the first is defined a-priori for the problem at hand by the user, the latter is not known and must be inferred directly from the data, reflecting the true underlying structure of the problem considered. To take this into account, we can soften the hierarchical relationships by allowing the matrices to take any value between 0 and 1. In this way, one microclass may be associated with multiple macroclasses with different confidences reflecting the semantic overlaps. To this purpose, we can define hierarchy joint distribution matrices $\mathbf{J}^{h_2, h_1} \in [0, 1]^{|\Omega^{h_2}| \times |\Omega^{h_1}|}$. Each term of the matrix $J_{i,j}^{h_2, h_1} = P(\omega_j^{h_1}, \omega_i^{h_2})$ models the probability of observing a relationship between microclass $\omega_i^{h_2}$ and macroclass $\omega_j^{h_1}$. This constraint relaxation allows us to better combine the *user-defined* aggregation problem with a *data-driven* centered architecture, by learning these matrices directly from the data.

D. Self-Supervised Hierarchical Consensus Learning

Let us return to the general case of H hierarchical levels, considering projections from source levels h to a target hierarchical level \tilde{h} . Each hierarchical level acts independently of the others. To ensure that the network is *hierarchy-aware*, an additional constraint based on the prediction associated to the target hierarchical level and the projected predictions from the other levels is defined. In particular, we take inspiration from the disagreement-based active learning field [25] to define the disagreement between the predictions calculated at each hierarchical level. For each level \tilde{h} , we consider a committee composed of all H levels. All predictions and their projected versions can be viewed as “soft” votes, which define each committee member’s confidence. Then, we introduce a self-supervised loss that penalizes the committee members’ disagreement with the overall committee consensus, thus guiding the learning of *data-driven* relationships in $\mathbf{J}^{h, \tilde{h}}$ and providing further supervision to the network based on the predictions at the different levels.

1) *Hierarchy-based Projected Predictions*: In order to generate the committee at each hierarchical level, the predictions first need to be projected to the other levels. For simplicity, let us consider the case of projection from source-level classes to target-level classes. Here we refer to estimated matrices as $\hat{\mathbf{J}}^{h, \tilde{h}} \in [0, 1]^{|\Omega^h| \times |\Omega^{\tilde{h}}|}$. The projected probability distribution $\hat{P}^{h \rightarrow \tilde{h}}(\omega_j^{\tilde{h}} | \mathbf{x})$ from source-level classes to target-level classes can be obtained from the probability distribution over the source-level classes $\hat{P}^h(\omega_i^h | \mathbf{x})$ and the hierarchy projection probabilities $\hat{P}(\omega_j^{\tilde{h}} | \omega_i^h)$ through the following relationship:

$$\hat{P}^{h \rightarrow \tilde{h}}(\omega_j^{\tilde{h}} | \mathbf{x}) = \sum_{i=1}^{|\Omega^h|} \hat{P}(\omega_j^{\tilde{h}} | \omega_i^h) \cdot \hat{P}^h(\omega_i^h | \mathbf{x}), \quad (7)$$

where the projection probabilities $\hat{P}(\omega_j^{\tilde{h}} | \omega_i^h)$ are directly derived by row-normalizing the estimated joint matrices $\hat{\mathbf{J}}^{h, \tilde{h}}$, i.e., we can define hierarchy projection matrices $\hat{\mathbf{M}}^{h, \tilde{h}} \in [0, 1]^{|\Omega^h| \times |\Omega^{\tilde{h}}|}$ such that $\hat{M}_{i,j}^{h, \tilde{h}} = \hat{P}(\omega_j^{\tilde{h}} | \omega_i^h)$. In general vector form, we can write the class-posterior probability vector $\hat{\mathbf{p}}^{h \rightarrow \tilde{h}}(\mathbf{x})$ projected from level h to level \tilde{h} as follows:

$$\hat{\mathbf{p}}^{h \rightarrow \tilde{h}}(\mathbf{x}) = (\hat{\mathbf{M}}^{h, \tilde{h}})^\top \cdot \hat{\mathbf{p}}^h(\mathbf{x}). \quad (8)$$

To ensure numerical stability and maintain better control over gradient magnitudes, we consider the computation of all the losses directly in the log domain. First, we compute the class-posterior log probabilities of classification modules \mathbf{g}^h from Eq. 2:

$$\log \hat{P}^h(\omega_i^h | \mathbf{x}) = g_i^h - \text{LSE}(\mathbf{g}^h), \quad (9)$$

where $\text{LSE} : \mathbb{R}^{|\Omega^h|} \rightarrow \mathbb{R}$ is the log-sum-exp (LSE) operator:

$$\text{LSE}(\mathbf{g}^h) = \log \sum_{i=1}^{|\Omega^h|} \exp(g_i^h). \quad (10)$$

Then, we can also define the projected predictions $\hat{P}^{h \rightarrow \tilde{h}}(\omega_j^{\tilde{h}} | \mathbf{x})$ from level h to level \tilde{h} in the log domain,

starting from the definition in the natural domain. Applying the logarithm to both sides of Eq. 7, we obtain the following:

$$\begin{aligned}
 \log \left(\hat{P}^{h \rightarrow \tilde{h}} \left(\omega_j^{\tilde{h}} | \mathbf{x} \right) \right) &= \\
 &= \log \left(\sum_i \hat{M}_{i,j}^{h,\tilde{h}} \cdot \hat{P}^h \left(\omega_i^h | \mathbf{x} \right) \right) \\
 &= \log \left(\sum_i \hat{M}_{i,j}^{h,\tilde{h}} \cdot \frac{\exp g_i^h}{\sum_k \exp g_k^h} \right) \\
 &= \log \left(\sum_i \exp \left(g_i^h + \log \hat{M}_{i,j}^{h,\tilde{h}} \right) \right) - \log \sum_k \exp g_k^h.
 \end{aligned} \tag{11}$$

This can finally be rewritten as the combination of two LSE operations, yielding the projected log-probability distribution at level \tilde{h} :

$$\begin{aligned}
 \log \left(P^{h \rightarrow \tilde{h}} \left(\omega_j^{\tilde{h}} | \mathbf{x} \right) \right) &= \\
 &= \text{LSE} \left(\mathbf{g}^h + \log \left(\hat{\mathbf{M}}_{:,j}^{h,\tilde{h}} \right) \right) - \text{LSE} \left(\mathbf{g}^h \right).
 \end{aligned} \tag{12}$$

To further simplify, hierarchy projection matrices can be defined directly in the log domain, *i.e.*, we learn log joint probabilities $\mathbf{L}^{h,\tilde{h}} = \log \hat{\mathbf{J}}^{h,\tilde{h}} \in \mathbb{R}^{|\Omega^h| \times |\Omega^{\tilde{h}}|}$. Then, we compute $\log \hat{\mathbf{M}}^{h,\tilde{h}}$ as follows:

$$\log \hat{\mathbf{M}}_{i,\cdot}^{h,\tilde{h}} = \mathbf{L}_{i,\cdot}^{h,\tilde{h}} - \text{LSE} \left(\mathbf{L}_{i,\cdot}^{h,\tilde{h}} \right), \tag{13}$$

which is equivalent to the row-normalization of $\hat{\mathbf{J}}^{h,\tilde{h}}$ in the log domain. The projected logits $\log \hat{\mathbf{p}}^{h \rightarrow \tilde{h}}$ can be used to calculate additional CCE losses that can contribute to the final loss [26]. However, this does not explicitly model the hierarchical consensus at the different hierarchical levels, requiring an additional step to ensure the joint classification of the classes.

2) *Semantics-Aware Hierarchical Consensus*: Given the projected prediction at each hierarchical level, we can now define a Hierarchical Consensus (HC) class probability vector $\hat{\mathbf{p}}_{HC}^{\tilde{h}}(\mathbf{x})$:

$$\begin{aligned}
 \hat{\mathbf{p}}_{HC}^{\tilde{h}}(\mathbf{x}) &= \\
 &= \frac{1}{Z^{\tilde{h}}} \sqrt[|\Omega^{\tilde{h}}|]{\hat{\mathbf{p}}^{\tilde{h}}(\mathbf{x}) \prod_{h \neq \tilde{h}} \hat{\mathbf{p}}^{h \rightarrow \tilde{h}}(\mathbf{x})} \\
 &= \frac{1}{Z^{\tilde{h}}} \sqrt[|\Omega^{\tilde{h}}|]{\hat{\mathbf{p}}^{\tilde{h}}(\mathbf{x}) \prod_{h \neq \tilde{h}} (\hat{\mathbf{M}}^{h,\tilde{h}})^{\top} \cdot \hat{\mathbf{p}}^h(\mathbf{x})},
 \end{aligned} \tag{14}$$

where $\hat{\mathbf{p}}_{HC}^{\tilde{h}}$ is the HC class-posterior probability defined as the geometric mean of the predictions at the target hierarchical level \tilde{h} and the projected predictions of all the other h levels, and $Z^{\tilde{h}}$ is a normalization constant to ensure that $\hat{\mathbf{p}}_{HC}^{\tilde{h}}$ sums

to one. This is equivalent to computing the average in the log domain [27]:

$$\begin{aligned}
 \hat{g}_{HC_j}^{\tilde{h}} &= \frac{1}{H} \left[\log \hat{P}^{\tilde{h}} \left(\omega_j^{\tilde{h}} | \mathbf{x} \right) + \sum_{h \neq \tilde{h}} \log \hat{P}^{h \rightarrow \tilde{h}} \left(\omega_j^{\tilde{h}} | \mathbf{x} \right) \right] \\
 &= \frac{1}{H} \left\{ \left[g_j^{\tilde{h}} - \text{LSE} \left(\mathbf{g}^{\tilde{h}} \right) \right] + \right. \\
 &\quad \left. + \sum_{h \neq \tilde{h}} \left[\text{LSE} \left(\mathbf{g}^h + \log \hat{\mathbf{M}}_{:,j}^{h,\tilde{h}} \right) - \text{LSE} \left(\mathbf{g}^h \right) \right] \right\}, \\
 \log \hat{\mathbf{p}}_{HC}^{\tilde{h}}(\mathbf{x}) &= \hat{\mathbf{g}}_{HC}^{\tilde{h}} - \text{LSE} \left(\hat{\mathbf{g}}_{HC}^{\tilde{h}} \right),
 \end{aligned} \tag{15}$$

where $\text{LSE}(\hat{\mathbf{g}}_{HC}^{\tilde{h}}) = \log Z^{\tilde{h}}$. While not directly supervised, HC can serve as an in-place replacement for the original classification modules during inference, providing a fully semantics-aware prediction in the downstream task.

3) *Self-Supervised Consensus Loss*: After calculating the consensus, both the prediction at the target level and the projected predictions are compared with the HC, defining an additional loss based on the divergence from the HC. To this purpose, we employ the JSD, which is defined as follows:

$$\begin{aligned}
 \text{JSD}^{h,\tilde{h}} \left(\hat{\mathbf{p}}_{HC}^{\tilde{h}} || \hat{\mathbf{p}}^{h \rightarrow \tilde{h}} \right) &= \\
 &= \frac{1}{2} \left(\text{KLD} \left(\hat{\mathbf{p}}_{HC}^{\tilde{h}} || \mathbf{q} \right) + \text{KLD} \left(\hat{\mathbf{p}}^{h \rightarrow \tilde{h}} || \mathbf{q} \right) \right),
 \end{aligned} \tag{16}$$

where \mathbf{q} is a mixture distribution of $\hat{\mathbf{p}}_{HC}^{\tilde{h}}$ and $\hat{\mathbf{p}}^{h \rightarrow \tilde{h}}$ calculated as $\mathbf{q} = \frac{1}{2}(\hat{\mathbf{p}}_{HC}^{\tilde{h}} + \hat{\mathbf{p}}^{h \rightarrow \tilde{h}})$, KLD represents the Kullback–Leibler divergence (KLD), and we omit the dependency on \mathbf{x} for simplicity. Please note that when $h = \tilde{h}$, we have that $\hat{\mathbf{p}}^{h \rightarrow \tilde{h}} = \hat{\mathbf{p}}^{\tilde{h}}$. Lastly, we can retrieve the JSD losses calculated at the different hierarchical levels and compute the final \mathcal{L}_{HC} penalty loss:

$$\mathcal{L}_{HC} = \frac{1}{N} \sum_{n=1}^N \sum_{\tilde{h}=1}^H \frac{1}{\log |\Omega^{\tilde{h}}|} \sum_{h=1}^H \text{JSD}^{h,\tilde{h}}(\mathbf{x}_n), \tag{17}$$

where the logarithm of the number of classes at level \tilde{h} , *i.e.*, $|\Omega^{\tilde{h}}|$, allows the balancing of the different number of classes at each hierarchical level. This prevents skewness towards levels with larger number of classes. The \mathcal{L}_{HC} measures the discrepancy between the HC prediction and the projected predictions, constraining the different layers to converge to the committee's vote.

E. Overall Loss Function

Lastly, the losses are averaged and summed to \mathcal{L}_{CCE} (Eq. 4):

$$\mathcal{L} = \mathcal{L}_{CCE} + \lambda_{HC} \mathcal{L}_{HC}, \tag{18}$$

where λ_{HC} is a metaparameters tuning the contribution of the HC loss. It is important to note that \mathcal{L}_{HC} does not require supervision, as it is simply a loss representing the divergence from the HC. Though the HC prediction is used within the

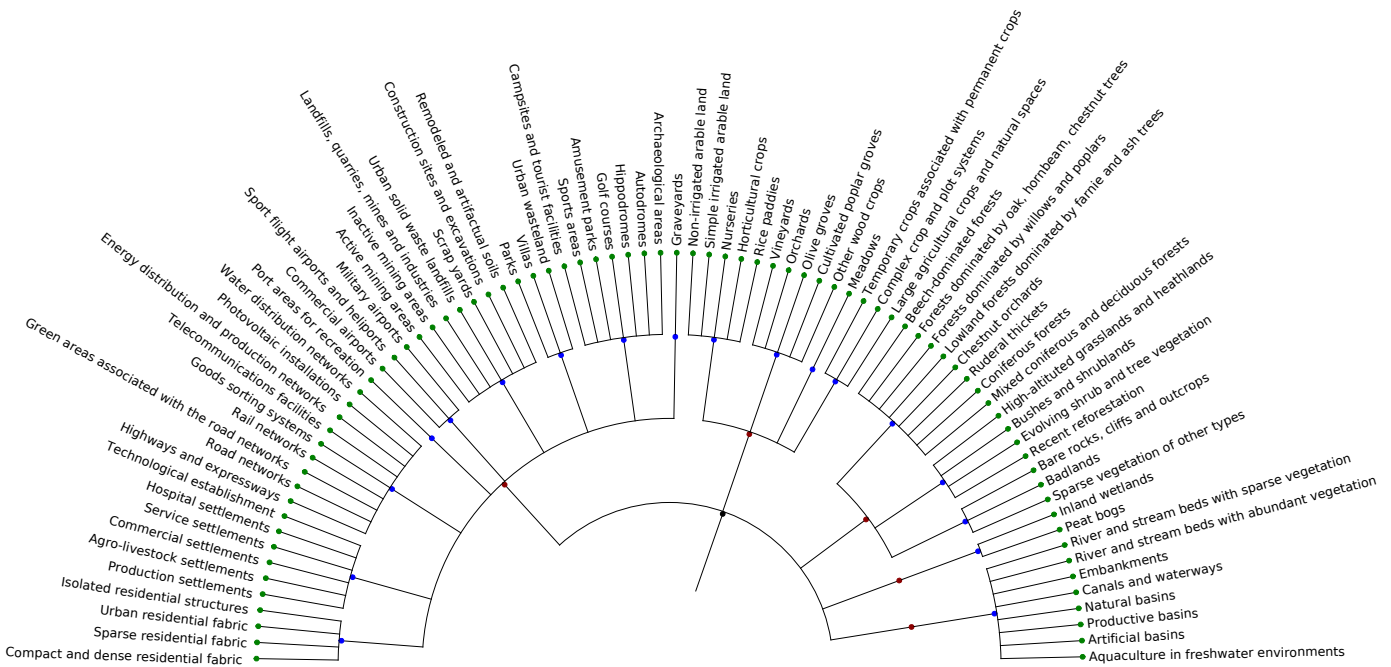


Fig. 3. A semicircular hierarchical label tree representation of the Emilia LU dataset at the fine-grained level of the hierarchy. The leaves corresponding to the fine-grained classes are shown in green, while the nodes for intermediate classes are depicted in blue, and those for coarse-grained classes are shown in red. The root node is represented in black.

penalty loss during the training phase, we consider the HC prediction at each hierarchical level as the final predictions for inference. This allows the architecture to leverage the semantic relationships learnt during the self-supervised training phase and to perform hierarchically consistent predictions.

IV. DATASET DESCRIPTION AND EXPERIMENT SETUP

This Section provides a description of the datasets employed in this study. Then, the experimental setup, including the pre-processing phase and the benchmark methodologies adopted for evaluating the DL models, are described.

A. NWPU-RESISC45

To assess the performance of the proposed methodology on VHR images, where spatial features play a prominent role, we considered the NWPU-RESISC45 [28] benchmark as a first dataset. NWPU-RESISC45 is composed of 31.500 RGB multi-resolution images for scene classification of VHR images categorized into 45 different classes at the finest-level of detail, and exhibits a high within-class diversity and between-class similarity. The dataset is completely balanced, *i.e.*, each class has the same number of samples at the *fine-grained* level. We defined a custom-hierarchy based on the subdivision defined in MillionAID [29], resulting in 8, 24, and 45 classes, corresponding to *coarse-grained*, *intermediate*, and *fine-grained* classes, respectively.

B. ELU Dataset

To further validate the performance of the proposed methodology, we additionally considered two multitemporal multispectral datasets differing in terms of complexity in the

hierarchical structure. The first dataset¹ consists of a publicly available LU map of 2020 over the Emilia Romagna region, Italy. The maps were defined considering the standard CORINE Land Cover (CLC) aggregation at three levels, with the third one further divided, resulting in an additional fourth level with an increased semantic detail. For the purpose of this analysis, we evaluated the hierarchical approach on three levels of hierarchy, consisting in the first two levels of the CLC and the additional finest level of detail, here referred to as *coarse-grained*, *intermediate* and *fine-grained*, respectively. The dataset has been built considering orthophotos and infrared images, and shows a minimum mapping unit of 0.16 hectares, with a minimum of 7m meters for linear structures. Although it has a good positional accuracy of 5m, the data may exhibit errors. Additionally, it represents LU classes, where the same Land-Cover (LC) class could be associated with different semantic classes, such as the fine-grained classes “Commercial airports”, “Sport flight airports and heliports”, and “Military airports”. We considered the Emilia Land Use (ELU) dataset corresponding to the Military Grid Reference System (MGRS) Sentinel-2 (S2) tile 32TPQ (10980 × 10980 pixels, for a total area of 110 × 110 km²). In the analyzed tile, the three hierarchical levels show 5, 18, and 80 classes at the coarse-grained, intermediate, and fine-grained levels, respectively. Please note that such an elevated number of fine-grained classes is not commonly approached in Earth Observation (EO) classification problems, where the majority of studies focus on the intermediate or coarse-grained classification task. Nonetheless, this level of precision allows a better monitoring of the class of interest and the extraction

¹Land Use of Emilia (2020). Accessed on May 13th 2025.

of information-rich content. Due to the high number of classes and, consequently, the large size of the hierarchical tree, we refer to this hierarchy as *a complex* hierarchy. A semicircular tree representing the hierarchical structure of the dataset is shown in Fig. 3.

C. ESA HRLC CCI Dataset

The second multitemporal multispectral dataset² has been derived under the High Resolution Land Cover (HRLC)-Climate Change Initiative (CCI) project by European Space Agency (ESA) [30]. The dataset includes LC classes organized according to the LCCS nomenclature, following the classification at the finest level of details. In this case, the hierarchical structure is less rigid compared to the Emilia dataset, as the classes are less detailed and can almost be considered independent. In this analysis, we use the HRLC10 maps, *i.e.*, the 10m resolution maps for the year 2019. The maps have been derived from machine learning approaches considering a joint approach based on multispectral (MS) S2 and Synthetic Aperture Radar (SAR) Sentinel-1 (S1) images [31]. The HRLC10 maps have been validated by intercomparison with other available maps and with photointerpreted samples. For our analysis, we considered the dataset corresponding to the MGRS S2 tile 22KGV (10980 × 10980 pixels, for a total area of 110 × 110 km²) in Brazil, mostly due to the heterogeneous presence of different classes. Since the hierarchical structure is simpler compared to the Emilia LU dataset, we defined three hierarchical levels ad-hoc, based on the similarity of the classes at the finest level of detail. This led to the definition of 3, 7, and 12 classes for the different levels, corresponding to *coarse-grained*, *intermediate*, and *fine-grained* classes, respectively. The coarse-grained classes have been divided in “Woody vegetated areas”, “Herbaceous vegetated areas”, and “Non-vegetated areas”. The fine-grained classes have been aggregated at the intermediate level considering the seasonality (*e.g.*, “Tree cover evergreen broadleaf” and “Tree cover deciduous broadleaf” are aggregated at intermediate level, while “Tree cover evergreen needleleaf” is still separated and aggregated at the coarse-grained level instead). Since the number of classes only shows a slight increment in the different layers, we refer to this hierarchy as *a simple* hierarchy.

D. S2 Preprocessing and Dataset Preparation

1) *VHR dataset*: The training, validation, and test splits were selected accordingly to [32], considering a split-ratio of 0.6, 0.2, and 0.2, respectively. During training, we applied data augmentation techniques consisting in resize, random crops and random rotations of the images.

2) *Multitemporal MS datasets*: The input data consists of S2 MS satellite images provided in the Copernicus EO program. The S2 acquisitions considered have been preprocessed at Level-2A (L2A) and re-projected at 10m/pixel resolution through a nearest neighbor approach. In the experiments, all

the bands except the 60m resolution band were used. Due to the high-complexity of both classification problems, we collected two time series (TS) of S2 images, fully exploiting the temporal signature and allowing the detection of seasonal targets. The S2 TS considered for the Emilia Dataset consists of acquisitions ranging from January 1st 2020 to December 31st 2020, while the S2 TS for the HRLC-CCI dataset consists of TS ranging from January 1st 2019 to December 31st 2019. Both the S2 TSs have been processed to achieve more regular TSs, resulting in 12 median monthly composites. This was achieved by computing the pixel-wise median for each band for each month. Before applying the median operator, we masked the samples associated with saturate or defective pixels, clouds, and cloud shadows. This approach allowed us to have regular, gap-free data in input to the DL models.

To extract a balanced training set, we considered an approach based on the heterogeneity of the input training patches. In particular, for both datasets, we divided the initial S2 monthly composite images into non-overlapping patches of 9 × 9 pixels. After the initial subdivision, we collected the patches and calculated the mode, extracting the dominant class of each patch analyzed. Then, the patches have been randomly subdivided into training, validation, and test sets, by considering a minimum number of N representative patches for each class in the analyzed classification scheme, with N fixed to 1000 for both the ELU and HRLC-CCI datasets. In the case of a minoritarian class had fewer patches than N , 50% of its total were assigned to the training set, 25% to the validation set, and 25% to the test set. In this way, we collected a small training dataset representative of the entirety of the classification scheme, corresponding to $\sim 1.35\%$ (1.631.616 pixels) and to $\sim 0.22\%$ (268.800 pixels) of the total number of patches in the tile for the Emilia Dataset and the HRLC-CCI dataset, respectively. The validation set size has been determined by considering 25% of the number of samples allocated for each class for the training set, while the remainder of the samples (*i.e.*, the entirety of the patches in the tile not belonging to the training and validation sets) have been used to validate the proposed approach in the test set.

E. Design of Experiments

Instead of validating the proposed hierarchical approach on a single backbone, we demonstrated its broad applicability by employing diverse backbone architectures representing different paradigms in a robust manner. All tests were conducted five times, with different random initializations of the weights of the architecture. For reproducibility, predefined seed values were used for the random number generator (RNG). The reported results include the values of Overall Accuracy (OA) for both tasks, while mean F1 Score (mF1) was also employed in the SITS MS classification task, along with the standard deviation (calculated as an unbiased estimator). For each architecture, we considered the following approaches: (i) the baseline with only the *fine-grained* classification through standard CCE minimization, (ii) the HAF method [18], (iii) the HRN module [20] and (iv) the proposed Semantics-Aware Hierarchical Consensus (SAHC). We removed the Granularity-

²ESA High-Resolution Land Cover Climate Change Initiative Project CEDA Archive site. Accessed on May 13th 2025.

Specific Block (GSB) block (two parameter-heavy convolutions and fully connected layers) from the HRN approach, maintaining only the hierarchical module. This is to ensure a fair comparison of architectures with the same number of parameters and focus solely on the hierarchical representation of the problem.

The different strategies are evaluated on the VHR scene classification task and the multitemporal MS semantic segmentation tasks. For the VHR task, we considered three different backbone architectures focusing on three different paradigms: (i) EfficientformerV2 S2 [33] for transformer-based architectures, (ii) MobileNetV2 [34] for CNN-based architectures, and (iii) LWGANet [35] for hybrid architectures. For the MS SITS classification task, we considered three different backbone architectures designed to process temporal information, also including hybrid architectures to further examine the effectiveness of the methodologies in utilizing contextual information: (i) the encoder part of a Transformer [36], (ii) an adaptation to the RS scenario of a *Swin Transformer* originally intended for super-resolution of videos [37], and (iii) a *Convolutional Long Short-Term Memory (ConvLSTM)* [38]. For a detailed description of the layer topology, please refer to the cited papers.

For each backbone, we replaced the classification head with three hierarchical classification heads, each characterized by a different level of granularity. We adopted the *AdamW* optimizer for all the architectures and configurations. The metaparameters of each different configuration have been validated considering a Tree-structured Parzen Estimator (TPE) algorithm to efficiently explore the search space. The learning rate and the weight decay were sampled from log-uniform distributions $U_{\log}([10^{-6}, 10^{-3}])$. Considering the proposed SAHC approach, the weight λ_{HC} associated to the HC loss has been sampled from a log-uniform distribution $U_{\log}([10^{-2}, 10^2])$, while the weights λ^h have been set empirically to 0.3, 0.2, and 0.5, to prioritize the fine-grained classification and reduce the influence of the intermediate and coarse-grained levels. To adjust the learning rate during training, we considered a cosine decay schedule. The weights associated to each model in the best performing epoch in terms of validation OA% and mF1% were used to conduct the inference on the test set, whose performance metrics are reported in the following section.

V. EXPERIMENTAL RESULTS

The experiments focus on validating the proposed SAHC approach over different backbones tasks, and datasets, comparing it to different standard and hierarchical approaches. We first focus on the results on the specific tasks, *i.e.*, scene classification on the VHR dataset and semantic segmentation of MS SITS. Then, we demonstrate the effectiveness of each component of the SAHC approach in an ablation study considering the ELU dataset. Finally, we analyze the trained hierarchy projection matrices to identify the key hierarchical relationships learnt by the proposed approach.

A. Case I: VHR Scene Classification

Table I shows the OAs of the LWGANet, MobileNet, and EfficientFormer on the NWPU-RESISC45 dataset. The

TABLE I
COMPARISON OF THE OVERALL ACCURACY OBTAINED BY DIFFERENT HIERARCHICAL METHODOLOGIES WITH DIFFERENT BACKBONE ARCHITECTURES ON THE NWPU-RESISC45 DATASET. THE BEST RESULTS ARE REPORTED IN BOLD, SECOND BEST ARE UNDERLINED. THE RELATED STANDARD DEVIATION IS REPORTED IN BRACKETS.

NWPU-RESISC45		
Backbone	Methodology	OA (%)
LWGANet L2 [35]	Baseline	92.50 (0.31)
	HAF [18]	<u>93.05 (0.29)</u>
	HRN [20]	93.01 (0.11)
	SAHC (proposed)	94.69 (0.18)
MobileNet V2 2.5× [34]	Baseline	<u>93.70 (0.30)</u>
	HAF	93.67 (0.28)
	HRN	93.58 (0.16)
	SAHC (proposed)	94.19 (0.33)
EfficientformerV2 S2 [33]	Baseline	90.41 (0.38)
	HAF	90.76 (0.46)
	HRN	<u>91.16 (0.44)</u>
	SAHC (proposed)	91.72 (0.14)

proposed SAHC achieves the best results, showing a higher OA% with all the different backbones. The HAF and HRN hierarchical modules show improvements only in the case of the transformer-based backbone (*i.e.*, EfficientFormer) and the hybrid backbone (*i.e.*, LWGANet), while the baseline approach without hierarchical modules performs better with the CNN-based approach (*i.e.*, MobileNet). In contrast, the proposed SAHC shows an increment in OA% of $\sim 1.2\%$ compared to the baseline approach with both the transformer-based and the CNN-based architectures, while exhibits a greater improvement when considering the hybrid backbone, with an additional $\sim 2.2\%$ increase in mF1%. These findings highlight the contribution of the hierarchical module. Indeed, its application to the hybrid architecture results in higher performance compared to its application to the CNN model. This result is particularly interesting given that the baseline CNN model outperforms the LWGANet baseline. It is also worth noting that, in most cases, the SAHC shows a smaller variability compared to its competitors, ensuring stabler results across different random initializations of the architecture weights.

B. Case II: MS SITS Semantic Segmentation

The second study case analyzes the semantic segmentation task, and is characterized by two different datasets with varying hierarchical complexity and differing label quality. The ELU dataset employs weak labels due to its focus on land use rather than land cover. Conversely, the HRLC-CCI dataset is designed for pixel-based LC classification, providing more precise and location-specific labels. Table II shows the performance of the three considered backbones on both the ELU and the HRLC-CCI dataset in terms of mF1% and OA%. The proposed approach outperforms the other methods on the ELU dataset, which exhibits stronger hierarchy and weaker labels than the HRLC-CCI dataset. Notably, the pixel-

TABLE II

COMPARISONS OF THE ACCURACIES OBTAINED BY DIFFERENT HIERARCHICAL METHODOLOGIES WITH DIFFERENT BACKBONE ARCHITECTURES ON THE ELU AND HRLC-CCI DATASETS. THE BEST RESULTS ARE REPORTED IN BOLD, SECOND BEST ARE UNDERLINED. THE RELATED STANDARD DEVIATION IS REPORTED IN BRACKETS.

Backbone	Methodology	ELU Dataset		HRLC-CCI Dataset	
		mF1 (%)	OA (%)	mF1 (%)	OA (%)
Swin Transformer [37]	Baseline (no hierarchy)	33.42 (0.44)	68.10 (0.65)	64.03 (1.06)	83.30 (1.22)
	HAF [18]	32.97 (0.57)	<u>68.15 (0.56)</u>	<u>64.26 (0.41)</u>	<u>83.35 (0.68)</u>
	HRN [20]	30.48 (0.86)	67.72 (1.98)	63.80 (0.38)	83.05 (0.49)
	SAHC (proposed)	34.57 (0.12)	71.25 (0.25)	66.49 (0.34)	84.75 (0.47)
Transformer [36]	Baseline (no hierarchy)	18.77 (0.29)	54.79 (0.87)	<u>61.14 (0.62)</u>	81.74 (0.72)
	HAF	19.04 (0.28)	55.69 (0.88)	61.12 (0.81)	81.37 (1.03)
	HRN	<u>20.97 (0.58)</u>	<u>57.48 (2.31)</u>	60.46 (1.05)	<u>81.80 (0.60)</u>
	SAHC (proposed)	25.63 (0.41)	65.94 (0.74)	64.07 (0.45)	83.30 (0.44)
ConvLSTM [38]	Baseline (no hierarchy)	25.82 (0.95)	<u>62.59 (0.70)</u>	65.19 (0.77)	84.32 (0.33)
	HAF	26.11 (0.92)	62.40 (0.57)	65.64 (0.84)	84.42 (0.68)
	HRN	25.53 (1.03)	62.36 (1.47)	65.18 (0.31)	84.19 (0.58)
	SAHC (proposed)	26.48 (0.35)	66.74 (0.42)	<u>65.38 (0.40)</u>	85.08 (0.28)

based transformer without contextual information shows an improvement of about 7% in terms of mF1% compared to the non-hierarchical baseline, while it also outperforms the other hierarchical approaches. In the case of the hybrid Swin Transformer and the ConvLSTM, the performance gap tends to decrease, while the adoption of the hierarchy and the consensus approach still shows an improvement. This result underlines the robustness of the proposed method to noisy labels, as the trained hierarchical matrices can learn soft hierarchical relationships directly from the data. In contrast, the compared methodologies rely on a hard hierarchy definitions, which might lead to suboptimal results in the case of labels that do not accurately represent the observed samples. The same behavior can be observed when analyzing the results on the HRLC-CCI dataset, where the hierarchy becomes weaker, but the real targets are better represented by the labels at the pixel level. In this case, the proposed approach performs similarly to the other methodologies, as the hierarchy is less noisy and the mapping more robust. Nonetheless, SAHC still outperforms the other methodologies, showing good generalization across the different backbones and scenarios. In our experiments, SAHC performed worse than HAF in terms of mF1% score only in the case of the ConvLSTM backbone, although the performance remains comparable. However, the proposed approach still shows a higher OA%, with reduced scores variability across different seeds. Lastly, Fig. 4 shows a visual comparison of the different hierarchical methodologies considering the HRLC-CCI dataset and the Swin Transformer backbone. From the qualitative results, one can see that the SAHC approach better represents the “Tree” classes, also showing a lower pixel-level noise.

TABLE III

ABLATION STUDY ON THE SWIN BACKBONE WITH THE ELU DATASET. THE CLASSIFICATION METRICS ARE REPORTED WITH THE RELATED STANDARD DEVIATION IN BRACKETS. THE BEST RESULTS ARE REPORTED IN BOLD, SECOND BEST ARE UNDERLINED.

Multi-level Classifiers	Hierarchical Consensus (Training)	Hierarchical Consensus (Inference)	mF1 (%)	OA (%)
			33.42 (0.44)	68.10 (0.65)
✓			33.48 (0.59)	68.10 (1.06)
✓		✓	<u>34.10 (0.41)</u>	67.83 (1.00)
✓	✓		33.48 (0.37)	<u>68.39 (0.33)</u>
✓	✓	✓	34.57 (0.12)	71.25 (0.25)

C. Ablation Study

The performance of each component in the proposed hierarchical approach is further analyzed in the ablation study presented in Table III. In this study, we evaluate the Swin backbone across five distinct configurations on the ELU dataset:

- 1) **Baseline**: the baseline approach with no multi-level classifiers;
- 2) **Multi-level**: the baseline approach augmented with additional classification heads for the coarse-grained and intermediate classes;
- 3) **Multi-level with HC inference**: the multi-level approach with consensus applied solely during inference (considering *user-defined* hierarchies);
- 4) **Multi-level with \mathcal{L}_{HC} training**: the multi-level approach trained with the self-supervised consensus loss, excluding consensus-based classification during inference;
- 5) **SAHC**: the proposed approach, which incorporates both the self-supervised consensus loss and consensus infer-

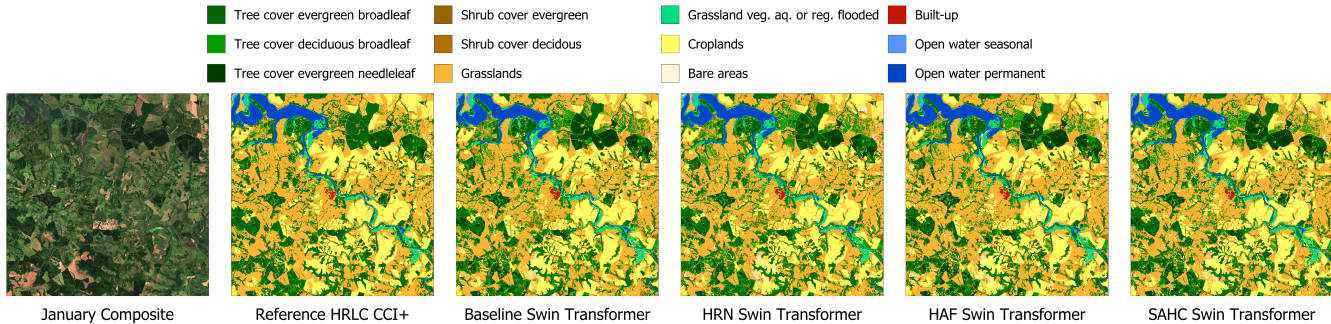


Fig. 4. Example of qualitative results at the fine-grained level on the HRLC-CCI dataset obtained by the considered methods using the Swin Transformer backbone.

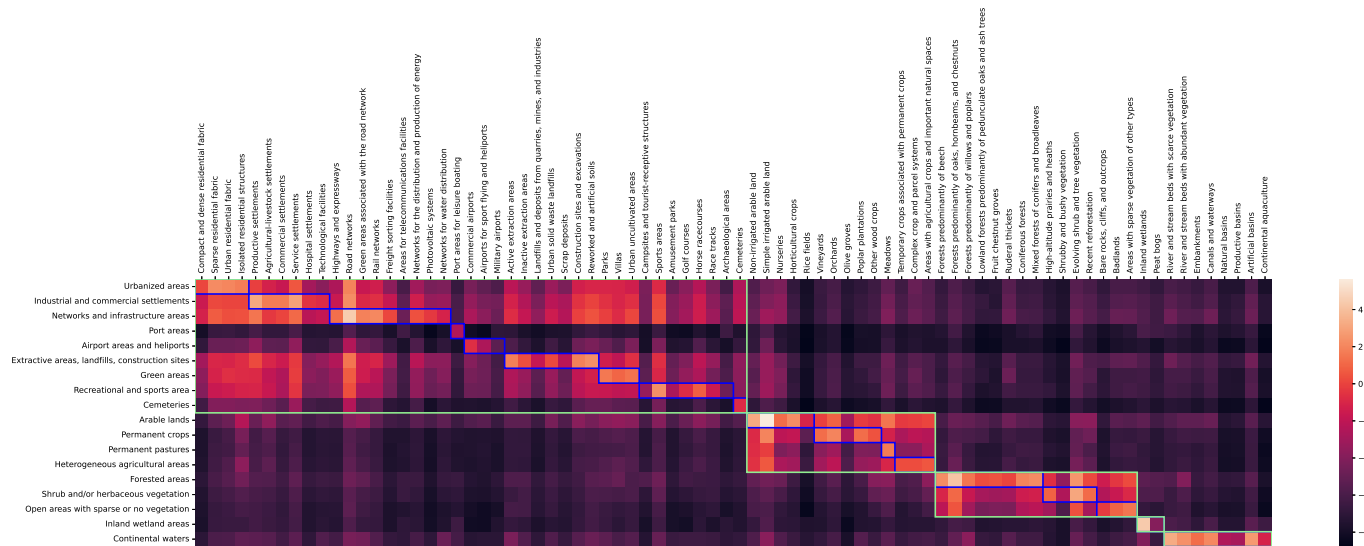


Fig. 5. Heatmap of the estimated hierarchy log-joint matrices considering the Swin Transformer backbone on the ELU dataset from fine-grained classes to intermediate classes. The blue and green rectangles identify the expected hierarchical aggregation of the fine-grained classes at the intermediate and coarse levels, respectively.

ence at multiple levels.

The table results indicate that incorporating multi-level classifiers into the baseline does not improve the overall performance. In fact, it leads to increased variability in the results, showing a higher variance and making the outcomes more unstable. However, the introduction of the HC inference improves the representation of fine-grained classes in terms of mF1%, also when considering the *user-defined* hierarchy in the multi-level approach with HC inference. On the contrary, the multi-level approach with \mathcal{L}_{HC} training does not improve the performance, as the JSD acts on the consensus across the layers and not on the fine-grained classification itself. This is instead addressed by the proposed SAHC, which combines the self-supervised consensus loss with consensus inference at multiple hierarchy levels. By allowing the trained matrices to learn the relationships from the data, the hierarchical consensus exhibits a sharp improvement in fine-grained classification, outperforming all other configurations. It is also important to note that the introduction of the JSD and the hierarchical consensus in inference leads to lower variance values, showing a more consistent *fine-grained* classification across different

weights initializations compared to the other approaches.

D. Hierarchy Projection Matrices Analysis

To better visualize the impact of the hierarchy projection matrices on classification results, we analyze the estimated hierarchy projection matrices of the Swin Transformer on the ELU and HRLC-CCI datasets. The visualization on the NWPU dataset is not reported as the hierarchical mappings show a trivial result, with perfect mapping of the defined hierarchical levels (mostly due to the simpler classification task).

Figure 5 presents a heatmap of the log-joint matrix between intermediate and fine-grained levels, highlighting the hierarchical structure captured by the proposed methodology on the ELU dataset. Note that the hierarchy projection matrix was uniformly initialized before training, with no prior knowledge of the *user-defined* hierarchical structure of the problem. The results show that the proposed approach effectively learns the hierarchy in the dataset. Specifically, the blue rectangles in the heatmap correspond to the user-defined expected mappings, from fine-grained classes to intermediate classes. Here, the

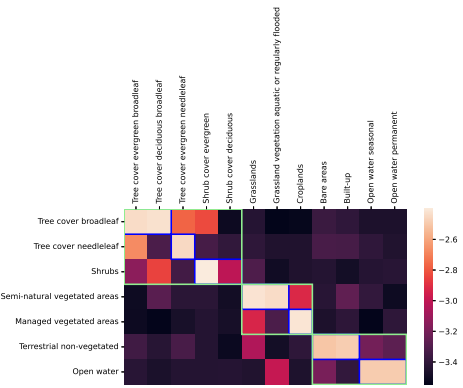


Fig. 6. Heatmap of the estimated hierarchy log-joint matrices considering the Swin Transformer backbone on the HRLC-CCI dataset from fine-grained classes to intermediate classes. The blue and green rectangles identify the expected hierarchical aggregation of the fine-grained classes at the intermediate and coarse levels, respectively.

weights associated to these mappings are highlighted, confirming that the *data-driven* estimated mappings are correctly following the *user-defined* hierarchies. Then, green rectangles indicate distant mappings to coarse-grained classes, revealing a similar pattern even though the matrix focuses on mappings between fine-grained and intermediate levels. It is important to note that separate hierarchy joint matrices are trained for the different hierarchical mappings in the proposed approach.

Similarly, Figure 6 depicts the heatmap associated with the HRLC-CCI dataset. As observed in the ELU case, the proposed methodology correctly extracts the hierarchy within the problem analyzed, emphasized by the blue rectangle showing the intermediate aggregation. However, the mappings appear more dispersed compared to the more complex ELU scenario, mostly due to the simpler hierarchical constraint leading to a smaller impact. Nonetheless, the trainable log-joint matrices allow soft-hierarchical mappings that were not considered in the initial *user-defined* hierarchy. One example can be observed in the weights associated to “Grassland vegetation aquatic or regularly flooded areas”, which shows an active semantic relationship with the “Open water” class, which is not mapped by the imposed *user-defined* hierarchy. This mapping highlights the importance of a data-driven approach, in contrast with the superimposition of a rigid hierarchical structures.

VI. CONCLUSION

In scene classification and semantic segmentation, the hierarchical relationship among the target classes is often under-exploited, resulting in the exclusion of valuable semantic information from the decision-making process. To address this limitation, this paper proposes the SAHC approach that leverages the hierarchical structure inherent in class types to improve the robustness and the accuracy of the classification. We introduced hierarchical classification branches, each designed to handle a specific hierarchical classification task, ranging from coarse-grained to fine-grained categories. Trainable hierarchy log-joint matrices are then defined to project the predictions across different hierarchical levels, following a

self-supervised data-driven approach which may not align with the rigid *user-defined* mappings between different hierarchy levels. This allows the implementation of a consensus mechanism, where predictions from multiple hierarchical levels are fused to perform the final decision. By progressively guiding the classification process from broader to specific categories, we can optimize the consensus, ensuring alignment among predictions at different hierarchical levels in a self-supervised fashion. The results show that *data-driven* hierarchies improve the performance at the finest level compared to directly using the *user-defined* hierarchies, contrarily to the performance drop usually observed in the literature when adding additional classification layers for different hierarchical levels after the backbone. The proposed methodology is both lightweight and scalable, making it easily adaptable to different architectures and datasets by simply reorganizing their structure in a hierarchical manner.

We evaluated the performance of the proposed approach on three different RS datasets. Indeed, the proposed approach is particularly relevant in VHR image and RS MS SITS classification, where the semantic structure of the data and available datasets support an explicit hierarchical representation of the task. The experimental results reveal that the proposed methodology is able to exploit both complex and simple hierarchies, demonstrating the best performances in terms of OA% and mF1% scores across experiments at the fine-grained hierarchical level. As expected, the improvements are particularly significant when complex hierarchies can be exploited within the RS data. The proposed method is general, showing top performance scores across different tasks and architectures.

A limitation of the proposed method is the reliance on a predefined hierarchy within the labels to train the self-supervised hierarchical consensus. While the consensus itself operates in a self-supervised manner, its training remains implicitly influenced by the supervised CCE losses at the coarser levels of the hierarchy. This predefined structure may not accurately represent the true underlying relationships within the data, potentially impairing model performance, or constraining the hierarchy log-joint matrices to learn a suboptimal representation of the hierarchical structure. To address this limitation, future research will explore methods for learning the hierarchical structure directly from the data. This approach would eliminate the need for manual definition of hierarchies, thereby improving the adaptability and accuracy of the model.

REFERENCES

- [1] J.-Y. He, S.-H. Liang, X. Wu, B. Zhao, and L. Zhang, “MGSeg: Multiple Granularity-Based Real-Time Semantic Segmentation Network,” *IEEE Trans. Image Process.*, vol. 30, pp. 7200–7214, Aug. 2021.
- [2] J. Wang, Q. Xu, B. Jiang, B. Luo, and J. Tang, “Multi-Granularity Part Sampling Attention for Fine-Grained Visual Classification,” *IEEE Trans. Image Process.*, vol. 33, pp. 4529–4542, Aug. 2024.
- [3] T. Yu, K. Fu, J. Zhang, Q. Huang, and J. Yu, “Multi-Granularity Contrastive Cross-Modal Collaborative Generation for End-to-End Long-Term Video Question Answering,” *IEEE Trans. Image Process.*, vol. 33, pp. 3115–3129, Apr. 2024.
- [4] Y. Zheng, J. Fan, J. Zhang, and X. Gao, “Exploiting Related and Unrelated Tasks for Hierarchical Metric Learning and Image Classification,” *IEEE Trans. Image Process.*, vol. 29, pp. 883–896, Sep. 2020.

- [5] J. Fan, N. Zhou, J. Peng, and L. Gao, "Hierarchical Learning of Tree Classifiers for Large-Scale Plant Species Identification," *IEEE Trans. Image Process.*, vol. 24, no. 11, pp. 4172–4184, Jul. 2015.
- [6] L. Li, T. Zhou, W. Wang, J. Li, and Y. Yang, "Deep hierarchical semantic segmentation," in *Proc. IEEE Conf. Comput. Vis. Pattern Recog.*, New Orleans, LA, USA, Jun. 2022, pp. 1236–1247.
- [7] T. Blaschke, "Object based image analysis for remote sensing," *ISPRS J. Photogramm. Remote Sens.*, vol. 65, no. 1, pp. 2–16, Jan. 2010.
- [8] E. Sertel, R. H. Topaloğlu, B. Şallı, I. Yay Algan, and G. A. Aksu, "Comparison of Landscape Metrics for Three Different Level Land Cover/Land Use Maps," *ISPRS Int. J. Geo-Inf.*, vol. 7, no. 10, p. 408, Oct. 2018.
- [9] G. Perantoni and L. Bruzzone, "Robust Training of Deep Neural Networks with Weakly Labelled Data," in *Signal and Image Processing for Remote Sensing*, C. H. Chen, Ed. Boca Raton, FL, USA: CRC Press, 2024, pp. 256–279.
- [10] Y. Wang, Y. Sun, X. Cao, Y. Wang, W. Zhang, and X. Cheng, "A review of regional and Global scale Land Use/Land Cover (LULC) mapping products generated from satellite remote sensing," *ISPRS J. Photogramm. Remote Sens.*, vol. 206, pp. 311–334, Dec. 2023.
- [11] X. Lu, Y. Chen, and X. Li, "Hierarchical Recurrent Neural Hashing for Image Retrieval With Hierarchical Convolutional Features," *IEEE Trans. Image Process.*, vol. 27, no. 1, pp. 106–120, Jan. 2018.
- [12] X. Li, D. Song, and Y. Dong, "Hierarchical Feature Fusion Network for Salient Object Detection," *IEEE Trans. Image Process.*, vol. 29, pp. 9165–9175, Sep. 2020.
- [13] A. Bilal, A. Jourabloo, M. Ye, X. Liu, and L. Ren, "Do Convolutional Neural Networks Learn Class Hierarchy?" *IEEE Trans. Vis. Comput. Graphics*, vol. 24, no. 1, pp. 152–162, Jan. 2018.
- [14] R. Cerri, R. C. Barros, and A. C. de Carvalho, "Hierarchical multi-label classification using local neural networks," *J. Comp. Sys. Sci.*, vol. 80, no. 1, pp. 39–56, Feb. 2014.
- [15] J. Fan, T. Zhao, Z. Kuang, Y. Zheng, J. Zhang, J. Yu, and J. Peng, "HD-MTL: Hierarchical Deep Multi-Task Learning for Large-Scale Visual Recognition," *IEEE Trans. Image Process.*, vol. 26, no. 4, pp. 1923–1938, Apr. 2017.
- [16] E. Giunchiglia and T. Lukasiewicz, "Coherent hierarchical multi-label classification networks," *Adv. Neural Inform. Process. Syst.*, vol. 33, pp. 9662–9673, Dec. 2020.
- [17] L. Bertinetto, R. Mueller, K. Tertikas, S. Samangooui, and N. A. Lord, "Making Better Mistakes: Leveraging Class Hierarchies With Deep Networks," in *Proc. IEEE Conf. Comput. Vis. Pattern Recog.*, Seattle, WA, USA, Jun. 2020, pp. 12 506–12 515.
- [18] A. Garg, D. Sani, and S. Anand, "Learning Hierarchy Aware Features for Reducing Mistake Severity," in *Proc. Eur. Conf. Comput. Vis.*, Tel Aviv, Israel, Oct. 2022, pp. 252–267.
- [19] J. Deng, N. Ding, Y. Jia, A. Frome, K. Murphy, S. Bengio, Y. Li, H. Neven, and H. Adam, "Large-scale object classification using label relation graphs," in *Proc. Eur. Conf. Comput. Vis.*, Zurich, Switzerland, Sep. 2014, pp. 48–64.
- [20] J. Chen, P. Wang, J. Liu, and Y. Qian, "Label Relation Graphs Enhanced Hierarchical Residual Network for Hierarchical Multi-Granularity Classification," in *Proc. IEEE Conf. Comput. Vis. Pattern Recog.*, New Orleans, LA, USA, Jun. 2022, pp. 4858–4867.
- [21] S. Illarionova, A. Trekin, V. Ignatiev, and I. Oseledets, "Neural-Based Hierarchical Approach for Detailed Dominant Forest Species Classification by Multispectral Satellite Imagery," *IEEE J. Sel. Topics Appl. Earth Observ. Remote Sens.*, vol. 14, pp. 1810–1820, Dec. 2021.
- [22] D. Ç. Demirkan, A. Koz, and H. Ş. Düzgün, "Hierarchical classification of sentinel 2-a images for land use and land cover mapping and its use for the CORINE system," *J. Appl. Remote Sens.*, vol. 14, no. 2, p. 026524, Jun. 2020.
- [23] A. Waśniewski, A. Hościło, and M. Chmielewska, "Can a Hierarchical Classification of Sentinel-2 Data Improve Land Cover Mapping?" *Remote Sens.*, vol. 14, no. 4, p. 989, Feb. 2022.
- [24] D. Chang, K. Pang, Y. Zheng, Z. Ma, Y.-Z. Song, and J. Guo, "Your 'Flamingo' is My 'Bird': Fine-Grained, or Not," in *Proc. IEEE Conf. Comput. Vis. Pattern Recog.*, Nashville, TN, USA, Jun. 2021, pp. 11 476–11 485.
- [25] B. Settles, *Active Learning*, ser. Synthesis Lectures on Artificial Intelligence and Machine Learning, R. J. Brachman, W. W. Cohen, and T. Dietterich, Eds. Cham, Switzerland: Springer, 2012.
- [26] G. Weikmann, G. Perantoni, and L. Bruzzone, "A class-driven hierarchical ResNet for classification of multispectral remote sensing images," in *Proc. SPIE Image Sign. Proc. Remote Sens. XXIX*, vol. 12733, Sep. 2023.
- [27] M. J. Rufo, J. Martín, and C. J. Pérez, "Log-Linear Pool to Combine Prior Distributions: A Suggestion for a Calibration-Based Approach," *Bayesian Anal.*, vol. 7, no. 2, pp. 411 – 438, Jun. 2012.
- [28] G. Cheng, J. Han, and X. Lu, "Remote Sensing Image Scene Classification: Benchmark and State of the Art," *Proc. IEEE*, vol. 105, no. 10, pp. 1865–1883, 2017.
- [29] Y. Long, G.-S. Xia, S. Li, W. Yang, M. Y. Yang, X. X. Zhu, L. Zhang, and D. Li, "On Creating Benchmark Dataset for Aerial Image Interpretation: Reviews, Guidances, and Million-AID," *IEEE J. Sel. Topics Appl. Earth Observ. Remote Sens.*, vol. 14, pp. 4205–4230, Apr. 2021.
- [30] L. Bruzzone, A. Amodio, F. Bovolo, M. A. Brovelli, M. Corsi, P. Defourny, P. Gamba, G. Moser, C. Otlé, L. P. Mayos *et al.*, "ESA-CCI High Resolution Land Cover: Generated Products," in *ESA Living Planet Symp.*, Bonn, Germany, May 2022.
- [31] L. Bruzzone, F. Bovolo, C. Paris, L. Maggiolo, P. Gamba, G. Moser, G. Perantoni, I. Podsiadlo, D. Solarna, T. Sorriso, M. Zanetti, and K. Meshkini, "ESA CCI High Resolution Land Cover: Methodology and EO Data Processing Chain," in *ESA Living Planet Symp.*, Bonn, Germany, May 2022.
- [32] M. Neumann, A. S. Pinto, X. Zhai, and N. Houlsby, "Training General Representations for Remote Sensing Using in-Domain Knowledge," in *Proc. IEEE Int. Geosci. Remote Sens. Symp.*, Waikoloa, HI, USA, Oct. 2020, pp. 6730–6733.
- [33] Y. Li, J. Hu, Y. Wen, G. Evangelidis, K. Salahi, Y. Wang, S. Tulyakov, and J. Ren, "Rethinking Vision Transformers for MobileNet Size and Speed," in *Proc. IEEE Int. Conf. Comput. Vis.*, Paris, France, Oct. 2023, pp. 16 889–16 900.
- [34] M. Sandler, A. Howard, M. Zhu, A. Zhmoginov, and L.-C. Chen, "MobileNetV2: Inverted Residuals and Linear Bottlenecks," in *Proc. IEEE Conf. Comput. Vis. Pattern Recog.*, Salt Lake City, UT, USA, Jun. 2018, pp. 4510–4520.
- [35] W. Lu, S.-B. Chen, C. H. Ding, J. Tang, and B. Luo, "LWGANet: A Lightweight Group Attention Backbone for Remote Sensing Visual Tasks," *arXiv:2501.10040*, 2025.
- [36] M. Rußwurm and M. Körner, "Self-attention for raw optical Satellite Time Series Classification," *ISPRS J. Photogramm. Remote Sens.*, vol. 169, pp. 421–435, Nov. 2020.
- [37] Z. Geng, L. Liang, T. Ding, and I. Zharkov, "RSTT: Real-time Spatial Temporal Transformer for Space-Time Video Super-Resolution," in *Proc. IEEE Conf. Comput. Vis. Pattern Recog.*, New Orleans, LA, USA, Jun. 2022, pp. 17 441–17 451.
- [38] S. Xingjian, Z. Chen, H. Wang, D.-Y. Yeung, W.-K. Wong, and W.-c. Woo, "Convolutional LSTM network: A machine learning approach for precipitation nowcasting," in *Adv. Neural Inform. Process. Syst.*, vol. 28, Montreal, Canada, Dec. 2015, pp. 802–810.